



Low equivalent weight short-side-chain perfluorosulfonic acid ionomers in fuel cell cathode catalyst layers

Chao Lei^a, Dmitri Bessarabov^{b,c}, Siyu Ye^d, Zhong Xie^a, Steven Holdcroft^{a,e}, Titichai Navessin^{a,*}

^a Institute for Fuel Cell Innovation, National Research Council Canada, Vancouver, BC, Canada V6T 1W5

^b Automotive Fuel Cell Cooperation, Burnaby, BC, Canada V5J 5J8

^c North-West University (NWU) and Council for Scientific and Industrial Research (CSIR), South African Hydrogen and Fuel Cell Program (DST-HySA), HySA Infrastructure Center of Competence, South Africa

^d Ballard Power Systems, Burnaby, BC, Canada V5J 5J8

^e Department of Chemistry, Simon Fraser University, Burnaby, BC, Canada V5A 1S6

ARTICLE INFO

Article history:

Received 26 January 2011

Received in revised form 10 March 2011

Accepted 12 March 2011

Available online 22 March 2011

Keywords:

Fuel cell

Catalyst layer

Short-side-chain ionomer

MEA

Equivalent weight

ABSTRACT

The morphology and fuel cell performance of cathode catalyst layers (CCLs) using low equivalent weight (EW) short-side-chain (SSC) perfluorosulfonic acid ionomers have been investigated in this work. The results were compared with those for a baseline CCL containing 30 wt% of the conventional ionomer 1100 EW Nafion[®]. The CCLs fabricated with 10–20 wt% of the Aquivion[™] ionomer displayed a similar morphology to the Nafion[®]-based CCLs. Electrochemical surface areas (ECSA) and double layer capacitances of all the Aquivion[™]-based samples were similar to those of the baseline. The oxygen reduction reaction (ORR) kinetics in CCLs with 20 wt% and 30 wt% Aquivion[™] were lower than the baseline under 100% relative humidity (RH), yet similar to the baseline at 70% RH. *In situ* electrochemical impedance spectroscopy (EIS) measurements suggested that the lowered ORR kinetics at 100% RH may be attributed to the large mass transport resistance in Aquivion[™]-based samples at low current densities. Relative to the baseline, CCLs containing 20 wt% Aquivion[™] ionomer demonstrated an improvement in fuel cell performance under operating conditions of 95 °C and RH values of 30, 50 and 70%. The greater hydrophilicity of the SSC ionomers is believed to account for the improved fuel cell performance at the relatively higher operating temperature and dry conditions.

Crown Copyright © 2011 Published by Elsevier B.V. All rights reserved.

1. Introduction

The membrane-electrode-assembly (MEA) plays an essential role in proton exchange membrane fuel cells (PEMFCs). The catalyst layers (CLs) of the MEA require effective three-phase reaction boundaries, high catalyst utilization, efficient conduction of protons and electrons, and facile transport of reactants and water throughout the entire electrode. The optimization of the electrode, especially the cathode catalyst layer (CCL) is essential for high fuel cell performance [1–3]. Perfluorosulfonic acid (PFSA) ionomers have been widely used as the electrolyte membrane and as a binder and proton conductor in CLs. The most commonly utilized ionomer is Nafion[®]; it consists of a polytetrafluoroethylene (PTFE) backbone and ether-linked, perfluorinated side chains with a sulfonic acid end group. Nafion[®] is often referred to as a long-side-chain (LSC) ionomer. To achieve good fuel cell performance, Nafion[®] is incorporated into the electrode to extend the three-phase reaction sites and

improve the pathway for proton conduction. A number of studies reveal that the optimal Nafion[®] loading in the CL is ~30 wt% [4–6].

Although Nafion[®] exhibits many advantageous properties and still remains a suitable material for fuel cell applications, it does have limitations; for example, the useful operating temperature is relatively low (<90 °C), and its proton conductivity is insufficient under dry conditions. For both stationary and automotive applications, it is desirable to operate fuel cells at higher temperatures (e.g. >100 °C) and under lower humidity conditions to improve reaction kinetics, enhance carbon monoxide tolerance at the anode, and simplify cooling and humidification subsystems [7].

A short-side-chain (SSC) PFSA ionomer, originally synthesized by Dow Chemical [8], showed an improvement in proton conductivity compared to Nafion[®] [9–12]. Due to the complexity of the synthetic process, the development of this SSC ionomer has been limited until recently. Solvay Solexis has developed a much simpler synthetic route and re-initiated the development of this SSC ionomer for fuel cell applications. The SSC ionomer is similar in structure to Nafion[®], however it contains a shorter pendant side-chain that carries the functional ion-exchange group. For a given equivalent weight (EW), SSC ionomers generally exhibit a higher

* Corresponding author.

E-mail address: titichai.navessin@nrc-cnrc.gc.ca (T. Navessin).

crystallinity and glass transition temperature when compared to Nafion®; these characteristics make SSC ionomers promising for high-temperature applications. Moreover, the enhanced crystallinity enables the EW of SSC membrane to be reduced to values as low as 700 g eq^{-1} , without having the membranes dissolve or swell excessively [9]. Compared with 1100 EW Nafion®, the SSC ionomer with an EW of 858 g eq^{-1} results in a higher charge carrier concentration, increased proton conductivity, and, thus, a smaller Ohmic potential loss [12]. A number of experimental and theoretical studies have been published on SSC PFSA membranes [10,13,14]; on the contrary, reports on using low EW SSC PFSA ionomers in the CCL remain scarce. Xu et al. have recently reported their results on improved PEMFC performance using low EW PFSA in the CCL; however, the study did not fully explore the microstructure–performance relationship from the perspective of electrode design [15]. Peron et al. studied the influence of different EW SSC ionomers on the cell performance at high temperatures, and found that fuel cell performance was greatly improved at 110 °C and 30% relative humidity (RH) [16]. Despite the above-mentioned findings reported in the literature, the role of SSC PFSA ionomers in CCLs is still not sufficiently understood.

Considering that the cell performance at low RH is strongly dependent on the water-uptake capacity of the ionomer in a CL, a systematic study on the microstructure–performance relationships of CCLs containing SSC ionomer is of particular interest. It is hypothesized that the low EW ionomer may reduce the ionomer loading requirements and change the structure of the CL. This potential structural change may possibly lead to a more effective use of pore space and improved cell performance. This work attempted to test and evaluate this hypothesis by preparing CCLs containing an 830 EW SSC ionomer (Aquivion™ D83-15C, Solvay Solexis). For comparison purposes, a baseline CCL was fabricated with an optimal Nafion® ionomer loading of 30 wt%. Various amounts of SSC ionomer were incorporated in the CCL, and the optimum SSC ionomer content was identified. The differences in morphology and electrochemical fuel cell performances between SSC-based MEAs and Nafion®-based MEAs are analyzed and discussed.

2. Experimental

2.1. Fabrication of membrane–electrode-assemblies (MEA)

Both cathode and anode catalyst inks were prepared using a dispersion media mixture of 1:1 MeOH/water and 46 wt% Pt/C (Tanaka Kikinokogyo). The solid content of all the inks was approximately 1 wt%. The Aquivion™ D83-15C SSC dispersion (EW 830, Solvay Solexis) was used as the CCL ionomer. The CCLs with various Aquivion™ contents, 10, 20, 30 and 40 wt%, are denoted as AQ10, AQ20, AQ30 and AQ40, respectively. CCLs with 30 wt% Nafion® ionomer (D-520, 5 wt% solution, EW 1100, DuPont) were also fabricated, and are denoted as NF30. The anode CL for all MEAs contained of 30 wt% Nafion® ionomer.

Nafion® membrane (25 μm thick, NRE-211, DuPont) was used as-received. An automated spray coater (EFD Ultra TT series) was employed to deposit the anode CL (0.1 mg cm^{-2} Pt) and the cathode CL (0.4 mg cm^{-2} Pt) onto the membrane. The catalyst-coated membranes (CCMs) had electrode geometrical surface areas of $5 \text{ cm} \times 5 \text{ cm}$. The membrane was mounted on a vacuum table heated to 85 °C. The anode CL was deposited first on one side of the membrane, and then the cathode CL was deposited on the other side. The amount of catalyst deposited was controlled by calibrating the flux of the spray coater; the calibration experiment consisted of spraying catalyst ink onto an inert substrate (Al foil) and measuring the mass deposited. The actual Pt loadings of cathode half-CCMs were verified by inductively coupled plasma–optical emission spec-

trometry (ICP-OES); the variation of the Pt loading was confirmed to be within 3% for a $0.40 \text{ mg Pt per cm}^2$ loading. Detailed fabrication procedures are described in the supplementary material of Ref. [3].

2.2. Physical characterization of catalyst inks and CCL

In order to assess the impact of ionomer on the catalyst ink dispersion and, thus, the ability to spray the CCL homogeneously, dynamic light scattering (Malvern Zetasizer Nano ZS) experiments were performed at 25 °C for more than 24 h on all the fresh inks. The inks containing different amounts of Aquivion™ ionomer provided similar particle size distributions. The mean, intensity-weighted, solvodynamic diameter of the prominent particles in the Aquivion™-based inks was similar to that of NF30 ink. The inks prepared using various loadings of Aquivion™ ionomer appeared to be stable for at least 24 h.

The morphology and cross-section of the prepared CCMs were examined using a scanning electron microscope (Hitachi S-3500N). The samples were prepared by fracturing the CCMs after immersion in liquid nitrogen. These fractured samples were then coated with gold by sputtering.

The peak pore size and pore size distribution (PSD) of the CCL were examined using a Hg porosimeter (Micromeritics, Auto Pore IV 9500). The applied pressure ranged from 177 to 3300 psi, corresponding to pore sizes of $1 \mu\text{m}$ to 5 nm in diameter. Detailed procedures are described in the supplementary material of Ref. [3].

2.3. MEAs and single cell

The CCM, which had a geometric area of 25 cm^2 , was inserted between two 24BC-type gas diffusion layers (SGL Group) and assembled into a single cell possessing straight flow-through channels. The uniformity of the cell compression was tested using pressure-sensitive films (Pressurex-Super Low, Sensor Products Inc.). The single cell was evaluated in a fuel cell test station (100 W, Scribner 850C, Scribner Associates, Inc.).

2.4. Fuel cell testing protocol

The MEAs were conditioned at 1.0 A cm^{-2} , 100% RH, 80 °C for at least 6 h and until the variation of the steady state potential was less than 1 mV. Air flowing at 5 SLPM and H_2 (purity 99.999%) flowing at 2 SLPM were used as the cathode and anode reactants, respectively.

Electrochemical surface area (ECSA) was measured by cyclic voltammetry (CV) using a potentiostat (1287A, Solartron Analytical). Humidified H_2 (0.5 SLPM, 80 °C) and N_2 (0.5 SLPM, 80 °C) were purged for 30 min at the anode and cathode, respectively. The N_2 flow was then set to zero, and the cell was stabilized for 20 min. Voltammograms were recorded under 0.5/0.0 SLPM H_2/N_2 using a 50 mV s^{-1} scan rate between 0.90 and 0.04 versus the anode. The final cycle of a set of 10 cycles was used for data analysis. The ECSA of MEAs was calculated from the integrated charge corresponding to the Pt–H desorption and adsorption peaks. The double-layer capacitance of the CCLs was also obtained from cyclic voltammograms.

The H_2 cross-over current density (i_{HX}) was measured by potential step voltammetry under constant 0.5/0.5 SLPM H_2/N_2 at the anode and cathode, respectively. The working electrode (cathode) potential was stepped from 0.2 to 0.5 V in 0.1 V increments and was equilibrated for 3 min.

In order to measure the ionic resistance in the CCL, electrochemical impedance spectroscopy (EIS) was performed using a Solartron 1287A potentiostat and a 1260 frequency analyzer. Flow conditions of 0.5/0.5 SLPM H_2/N_2 were used once again. The amplitude of the sinusoidal current signal for the AC impedance was set at

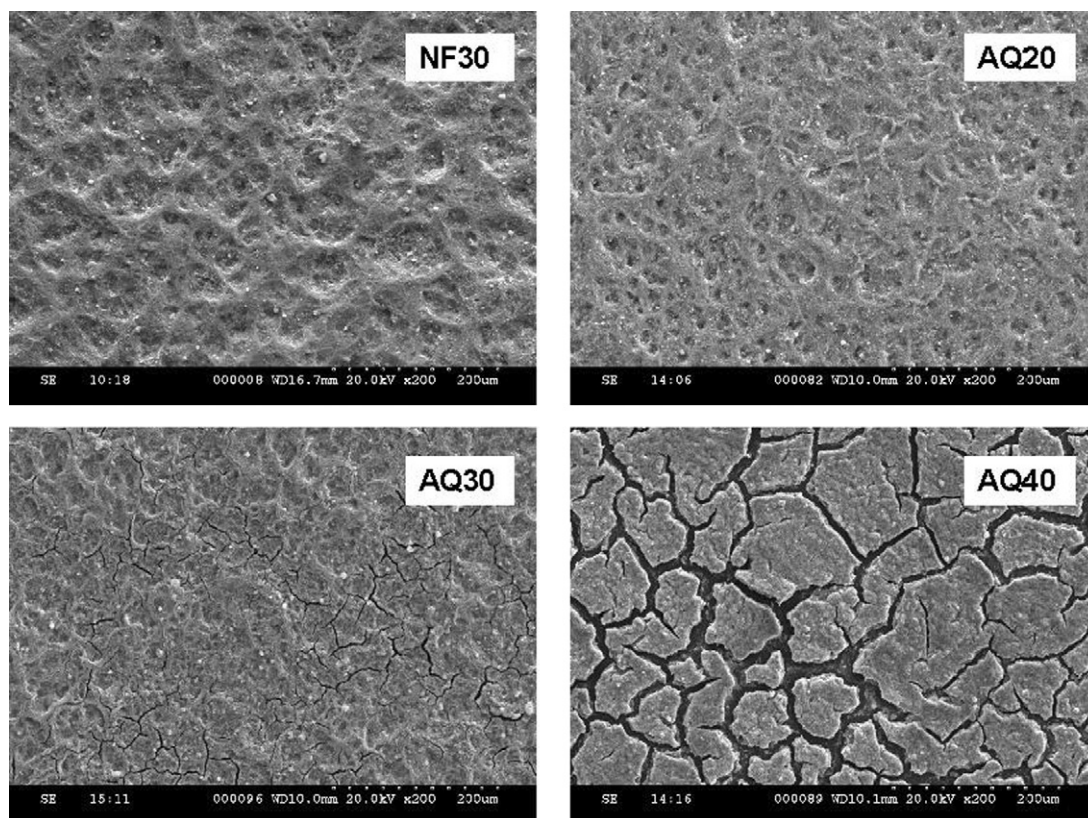


Fig. 1. SEM images of the top surface of CCLs under 200 \times magnification.

10 mV over a frequency range of 20 kHz to 0.1 Hz. EIS spectra were obtained under a DC bias potential of 0.45 V versus the anode.

The ORR kinetics of these CCLs were determined by acquiring H_2/O_2 polarization curves at 100% and 70% RH using excessive gas flow rates of 2 SLPM H_2 and 5 SLPM O_2 . The current load gradually decreased in intervals from 1 A cm^{-2} to 0.008 A cm^{-2} and was held for 15 min at each point. The cell potential at steady state was obtained by averaging the data recorded in the last 2 min. The cell potentials were plotted against the log of current density, and the Tafel slope was extracted.

Beginning of life (BOL) cell performance of these MEAs were evaluated at 80 and 95 $^{\circ}C$ under different relative humidities (100%, 70%, 50% and 30% for both anode and cathode) at ambient pressure. The H_2 /air polarization curve was obtained galvanostatically, and the cell was held at each current load for 10 min to reach a steady state in which the potential variation was less than 1 mV. The cell potential was obtained by averaging the data in the last 2 min. EIS experiments were conducted by imposing a small sinusoidal (AC) voltage of known amplitude and frequency on the cell, while monitoring the cell's amplitude and phase response. The perturbation amplitude for the AC impedance was 10% of the direct current over a frequency range of 10 kHz to 0.1 Hz.

3. Results and discussion

3.1. Morphology and thickness of the CCLs

Fig. 1 shows SEM images of the top surface of the various CCLs prepared. Sample AQ10 (not shown), AQ20 and the baseline CCL, NF30, all displayed a similar dense surface. As the content of AquivionTM in the CL was increased from 20 to 30 wt%, cracks appeared in the catalyst layer. The cracks in AQ40 had widths up to 20 μm and were large enough to separate the CLs into islands.

In fact, cross-sectional micrographs (Fig. 2) suggested that these cracks penetrated the entire thickness of the CL. The thickness of the different CL samples is summarized in Table 1. All the AquivionTM-based CLs show a uniform thickness of about $11 \pm 2 \mu m$.

It is noteworthy that, by using the same ink formulation and fabrication parameters, the formation of micro-cracks has not been observed in CLs containing high Nafion[®] contents of up to 40 and 50 wt% in our study. In an attempt to avoid the formation of cracks in the CLs containing the AquivionTM ionomer, modifications to the following fabrication parameters were evaluated: heating temperature and evaporation rates (increasing the substrate temperature from 70 to 88 $^{\circ}C$), catalyst materials (employing different types of carbon supported Pt), and the substrates (depositing on membrane or Al foil). These parameters provided negligible change in the observed microstructure. This evaluation leads to a consideration that the formation of micro-cracks in the AquivionTM-based CLs may be due to the high hydrophilicity of low EW ionomers [17] and the use of water-based ink formulations.

The peak pore size and PSD (Fig. 3) of the CLs were examined by Hg porosimetry. The porosities based on cumulative intrusion are listed in Table 1. In general, the PSD of the samples AQ20 and AQ30 ranged from 10 to 400 nm, and were similar to that of NF30. AQ40 displayed a very low pore volume with pore sizes in the range from 5 to 10 nm. Since the porosity results from a typical Hg porosimeter only account for the pore volume associated with pore sizes

Table 1
Thickness and porosity of CCLs.

	NF30	AQ10	AQ20	AQ30	AQ40
Thickness of CL (μm)	10.5	11.0	11.0	11.5	11.0
Thickness deviation (μm)	± 2.0	± 1.0	± 2.0	± 2.0	± 1.0
Peak pore size (nm)	~ 50	~ 35	~ 40	~ 40	/
Porosity (%)	~ 38	~ 47	~ 42	~ 21	~ 8

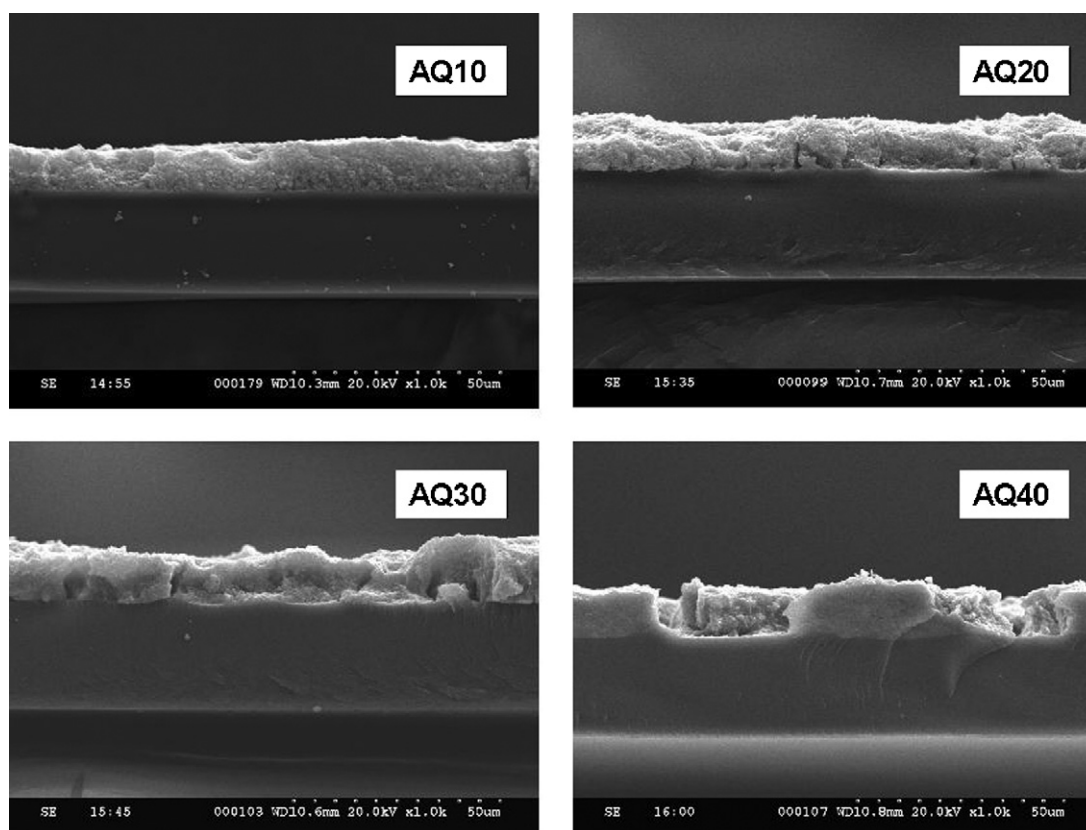


Fig. 2. Cross sectional SEM images of CCLs under 1k \times magnification.

less than 1 μm [3], the porosity of sample AQ30 may have been underestimated due to its micro-cracks. As shown in Fig. 1, some of these cracks have widths and lengths larger than 1 μm , and, therefore, they may not have been included in the calculated porosity. It was found that both the porosity and the range of PSD profile of AquivionTM-based CLs decreased as the AquivionTM content increased. This trend indicates that the ionomer penetrated both meso- (2–50 nm diameter) and macro- (>50 nm diameter) pores. It was expected that the CL sample with extensive micro-cracks and low porosity may exhibit insufficient reproducibility and high activation polarization losses during electrochemical characterization [18,19]; therefore, AQ40 was not included for further systematic investigation.

3.2. Electrochemical fuel cell analysis and discussion

Cyclic voltammograms of different CCLs in MEAs at 80 $^{\circ}\text{C}$ and 100% RH are shown in Fig. 4. The AquivionTM-based CCLs exhibit characteristic features of hydrogen adsorption/desorption and oxide formation/reduction that are similar amongst themselves and when compared to the baseline CCL NF30. The ECSA data and double layer capacitances (C_{dl}) under the above-mentioned conditions are summarized in Table 2. The ECSA and C_{dl} values for the

Table 2
Electrochemical performance at 80 $^{\circ}\text{C}$ and 100% RH of MEAs prepared with various CCLs.

	ESA (H-des) ($\text{m}^2 \text{g}^{-1}$)	ESA (H-ads) ($\text{m}^2 \text{g}^{-1}$)	C_{dl} (mF cm^{-2})	i_{HX} (mA cm^{-2})
NF30	40.7	42.9	19.3	2.07
AQ10	39.1	39.2	24.1	1.78
AQ20	41.5	41.7	18.7	1.92
AQ30	41.1	43.3	19.3	1.70

AquivionTM-based CCLs were close to those for NF30, indicating that the surface area of Pt in contact with ionomer was similar for the Nafion[®] and AquivionTM-based samples analyzed.

H_2 cross-over currents for all the tested MEAs were found to be less than 2.1 mA cm^{-2} (Table 2), and accounted for less than 4% of the current density of a fuel cell operating under practical conditions (0.8–0.3 V, 0.06–1.40 A cm^{-2} , see polarization curves below). Therefore, the loss of efficiency caused by H_2 cross-over could be considered negligible.

The proton conductivities of the CLs were evaluated by EIS under an operating temperature of 80 $^{\circ}\text{C}$ and with RH values of 70% and 100%. Impedance spectra are presented as Nyquist plots in Fig. 5. For clarity, the spectra are shifted to the origin by removing high frequency resistance from the real axis. As expected and under both operating conditions, the proton resistance (R_p) of the CL decreased with the increasing content of AquivionTM, the proton conductor, in the CCL. In comparison to NF30, AQ10 exhibited a higher proton resistance of the CL, whereas AQ20 demonstrated a similar proton resistance of the CL despite its relatively lower ionomer content. At the same ionomer loading, AQ30 exhibited a lower proton resistance of the CL than the baseline NF30. These results suggest that the low EW (high ion exchange capacity) ionomer reduces the required ionomer loading in the CLs, while maintaining adequate electrode proton conductivity.

H_2/O_2 polarization curves of MEAs were recorded using an operating temperature of 80 $^{\circ}\text{C}$, RH values of 70% and 100%, and excessive gas flow rates. Tafel plots were constructed and are shown in Fig. 6. In order to compare the results, the iR_u -corrected electrode potentials (defined as the measured potential plus the iR_u compensation) were plotted against the compensated current density (measured current density plus the cross-over current density). In the kinetically controlled regime ($E > 0.80 \text{ V}$) under fully humidified conditions, the Tafel slopes for AquivionTM-based MEAs

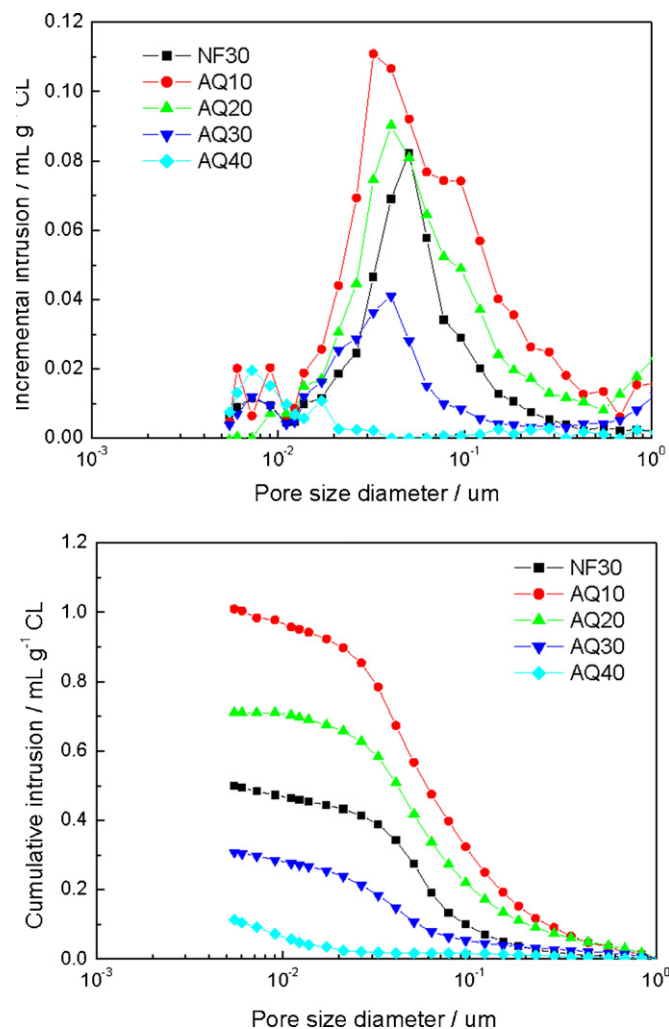


Fig. 3. Pore size distribution of the half-CCMs.

increased as the ionomer content is increased. AQ20 and AQ30 showed higher Tafel slopes ($82\text{--}86\text{ mV dec}^{-1}$) than the baseline NF30 CCL (63 mV dec^{-1}); however, when the RH was decreased to 70%, AQ20 and AQ30 MEAs displayed similar Tafel slopes

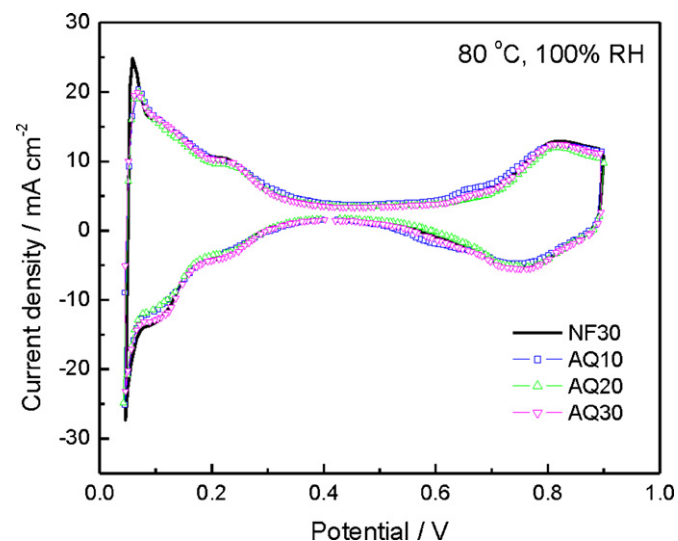


Fig. 4. Typical cyclic voltammograms of CCLs in MEAs at $80\text{ }^{\circ}\text{C}$ and 100% RH.

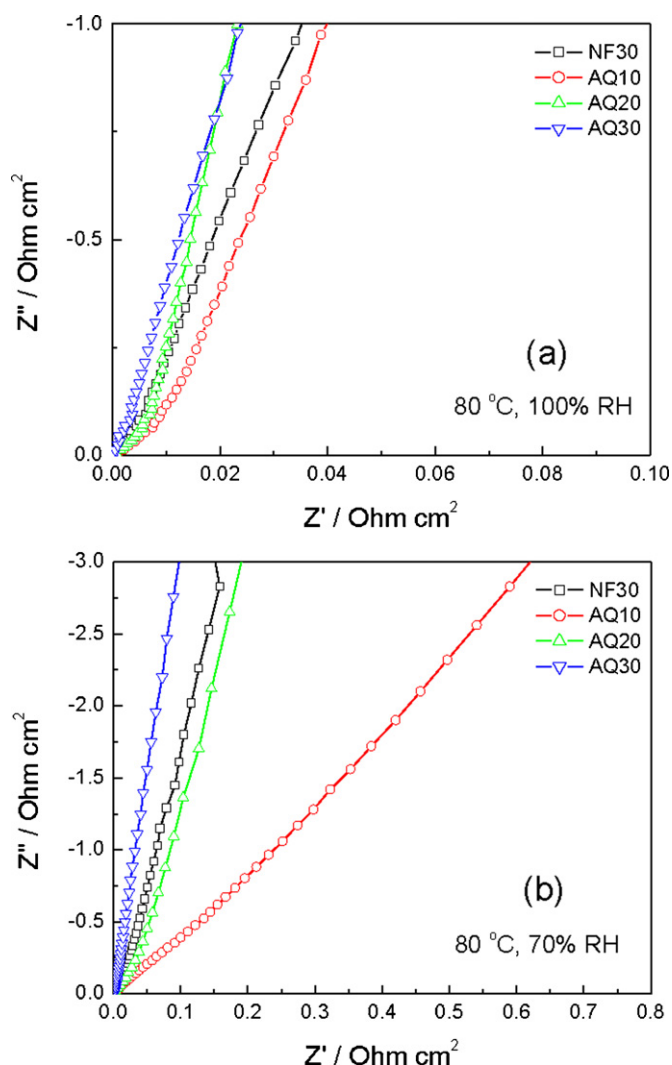


Fig. 5. Nyquist plots of CCLs in MEAs under operating conditions of $80\text{ }^{\circ}\text{C}$ and RH values of (a) 100% and (b) 70%.

($61 \pm 1\text{ mV dec}^{-1}$) to NF30 (65 mV dec^{-1}). This similarity implied that these different CCLs demonstrated the same inherent electrode kinetics towards ORR at 70% RH. The slightly higher Tafel slope of approximately 78 mV dec^{-1} for AQ10 at 70% RH can be attributed to its higher proton resistance [see Fig. 5(b)]. It is commonly observed that the Tafel slope for CCLs containing Nafion® remains constant when the ionomer is sufficiently hydrated, i.e., at RH values above 60–70% [20,21]. This trend was also seen in this study, as the baseline NF30 sample's Tafel slope remained almost constant as the RH was changed from 70% to 100%. Such a trend did not exist for the CCLs containing the Aquivion™ ionomer: AQ20 and AQ30 exhibited higher Tafel slopes at 100% RH, indicating that their ORR activities were reduced.

In order to further understand the different electrode kinetics, *in situ* EIS was performed at 0.05 A cm^{-2} and under H_2/air operating conditions. Impedance plots are shown in Fig. 7. For clarity of comparison, the high frequency intercepts, which represent the uncompensated Ohmic resistances, are offset to zero. The low frequency intercept on the real impedance axis (R_{if}), i.e., the diameter of the semi-circle, corresponds to the sum of the effective charge transfer resistance (R_{ct}) and mass transport resistance (R_{mt}). At very low current densities, it was assumed that there are no significant losses associated with delivery of reactant gases to the electrode interface since the oxygen consumption rate is small; therefore, R_{if}

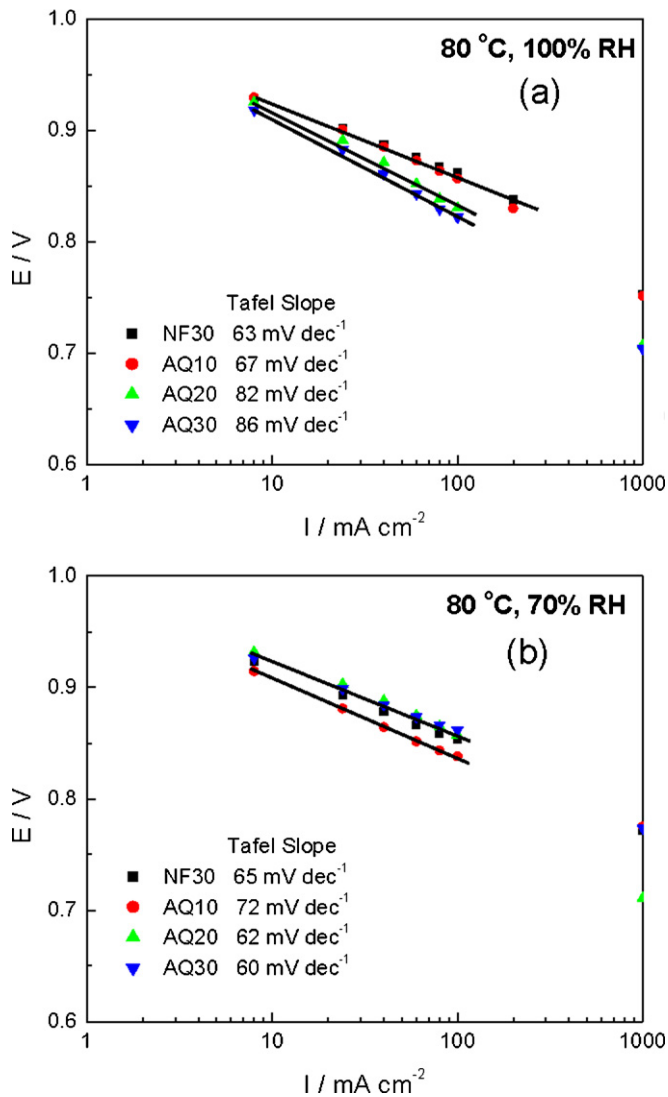


Fig. 6. Tafel plots of H_2/O_2 polarization at $80^\circ C$ and RH values of (a) 100% and (b) 70%.

was mainly attributed to R_{ct} . It was found that, as the RH changes from 70% to 100%, the R_{if} for NF30 remained nearly constant and the R_{if} for AQ10 decreased slightly. On the contrary, the R_{if} for AQ20 and AQ30, which were similar at 70% RH, increased dramatically under fully humidified conditions. The observed trends for R_{if} are consistent with the Tafel slope analysis; thus indicating that the lowered ORR kinetics in AQ20 and AQ30 can be attributed to the larger resistance, R_{if} . Given that the MEA fabrication and testing protocols were the same for all the samples, the increase in R_{if} (or lowered ORR kinetics) for AQ20 and AQ30 under the fully humidification condition may be related to the intrinsic properties of the SSC ionomer. We speculate that the higher hydrophilicity of the Aquivion™ ionomer than Nafion® leads to a higher water content in the ionomer network. Under the fully humidified condition, this augmented water content could possibly have two deleterious effects: (i) dilution of the local proton concentration, and (ii) reduction of the solubility of oxygen in the ionomer. Further detailed investigations are required to fully understand the observed phenomena.

The H_2 /air polarization curves obtained at $80^\circ C$ and 100% RH, as well as the contribution from the Ohmic resistance, are plotted in Fig. 8. The high frequency resistance (HFR), which predominantly consists of the membrane's ionic resistance and other

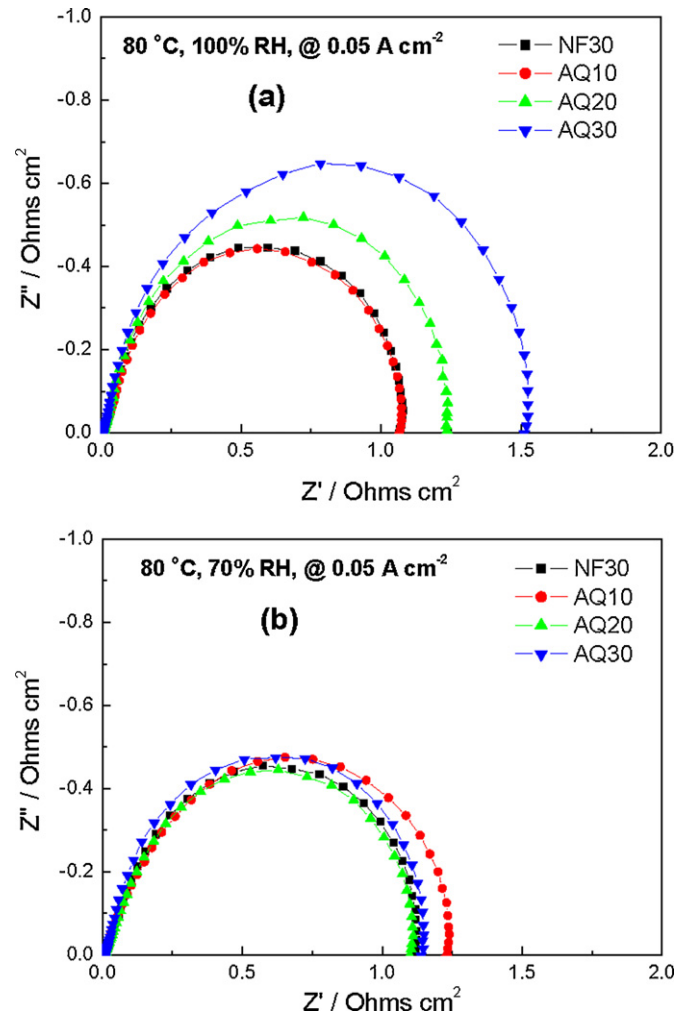


Fig. 7. *In situ* electrochemical impedance spectra obtained at $80^\circ C$, $0.05 A cm^{-2}$, and RH values of (a) 100% and (b) 70%.

electronic/contact resistances, were very similar for all CCL samples. In the kinetic region, the cell performances of AQ20 and AQ30 were lower than that of NF30, while the performance of AQ10 is similar to the baseline. These observations are consistent with the Tafel slope analysis and the EIS results presented in Figs. 6 and 7, respectively.

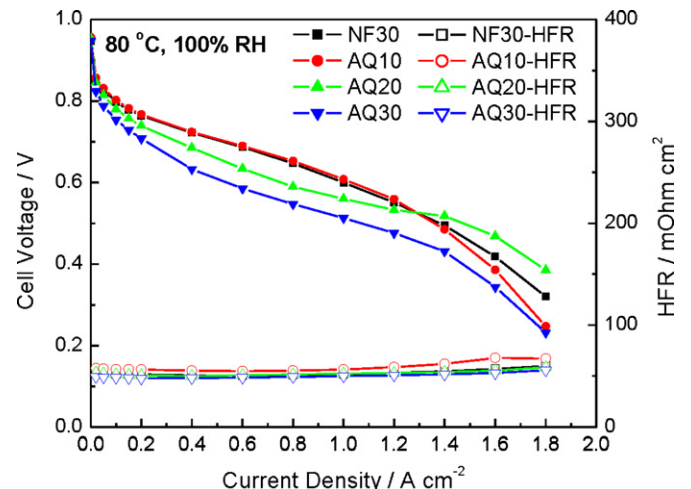


Fig. 8. H_2 /air polarization curves at $80^\circ C$ and 100% RH.

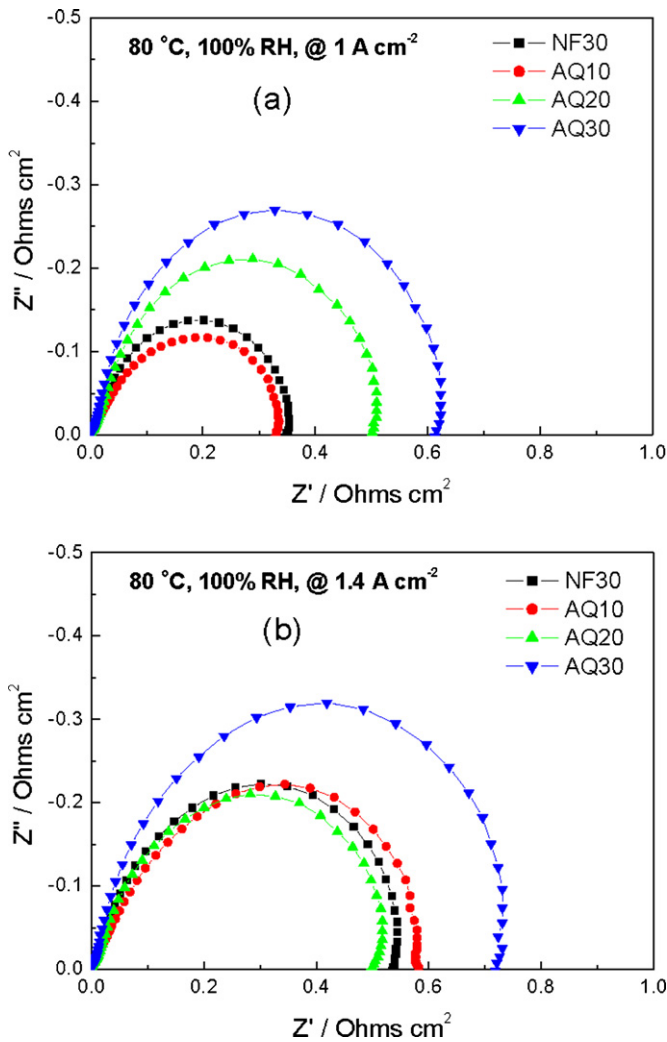


Fig. 9. *In situ* electrochemical impedance spectra obtained at 80 °C and 100% RH while the cell is operated at (a) 1.0 A cm⁻² and (b) 1.4 A cm⁻².

In the mass transport region (current densities >1.0 A cm⁻²), the trend of the polarization curves was complex. AQ10 mimicked the performance behaviour of the NF30 baseline at current densities <1.4 A cm⁻², but demonstrated slightly lower performance at >1.4 A cm⁻². AQ20 showed an improvement in the mass transport region relative to AQ10 and exhibited a higher performance than the baseline at >1.4 A cm⁻². *In situ* EIS data were recorded at 100% RH while the cell was operated at two different current densities (Fig. 9). When the current density was raised from 1.0 to 1.4 A cm⁻², the R_{if} for NF30 increased from 0.350 to 0.525 Ω cm⁻². A similarly large increase from 0.325 to 0.575 Ω cm⁻² was exhibited by the R_{if} for AQ10. As seen for NF30 and AQ10, at high current densities, R_{if} is expected to increase with increasing current density because of the exacerbated mass transport limitations. Surprisingly, only a small increase in R_{if} from 0.625 to 0.700 Ω cm⁻² was observed for AQ30, while the R_{if} for AQ20 remains essentially unchanged at 0.500 Ω cm⁻². The results of the EIS data were consistent with performance behaviours demonstrated at current densities >1.0 A cm⁻². The exceptional trends of R_{if} for AQ20 and AQ30 are speculated to be related to an envisioned reduction in catalyst layer flooding and warrant further investigation.

At 70% RH and 80 °C, the Aquivion™-based MEAs displayed smooth polarization curves, as shown in Fig. 10. At the low current densities of the kinetically controlled region, AQ20 and AQ30 achieved the same cell voltages as the baseline NF30, while AQ10

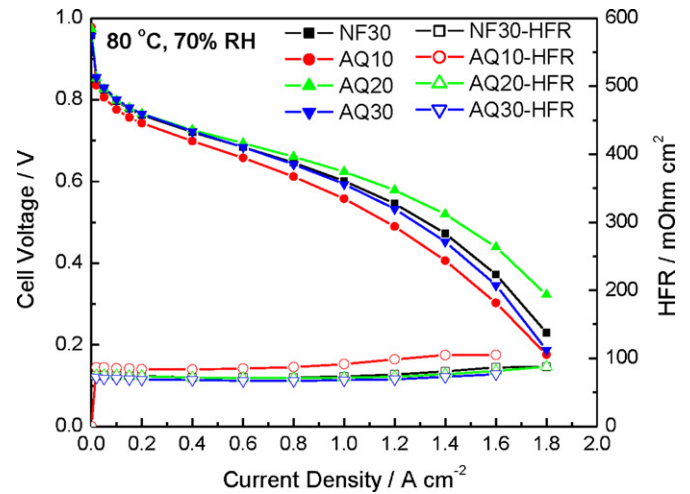


Fig. 10. H₂/air polarization curves at 80 °C and 70% RH.

showed slightly lowered cell potentials. These results were also consistent with the ORR kinetic data reported in Fig. 6. At higher current densities, each of the Aquivion™-based MEAs demonstrated a different trend relative to NF30. The cell voltage of AQ10 remained slightly lower than NF30. The performance of AQ30 was quite similar to the baseline sample; for example, the difference in potential at 1 A cm⁻² was less than 10 mV. Moreover, AQ20 exhibited a higher performance than NF30. The performance improvement of AQ20, in comparison to NF30, was more pronounced at higher current density; for example, the magnitude of the enhanced performance grew from 26 mV at 1.0 A cm⁻² to 52 mV at 1.4 A cm⁻².

In order to more fully understand the cell performance at 80 °C and 70% RH, *in situ* EIS were obtained for the MEAs while at 1.0 A cm⁻² (Fig. 11). The spectrum for each MEA consisted of two distinct impedance arcs, corresponding to R_{ct} at high frequency and R_{mt} at low frequency. As previously discussed, R_{ct} , which is determined by ORR kinetics, was similar for AQ20, AQ30 and NF30 [see Figs. 6(b) and 7(b)]. The difference in the impedance spectra of these three MEAs is attributed to R_{mt} . AQ20 displayed the smallest R_{mt} and, thus, the lowest total cell resistance, which accounts for its superior performance. It is noteworthy that the trend of increasing R_{mt} of these three samples is consistent with their decreasing porosity results (see Section 3.1). AQ10 had the highest porosity

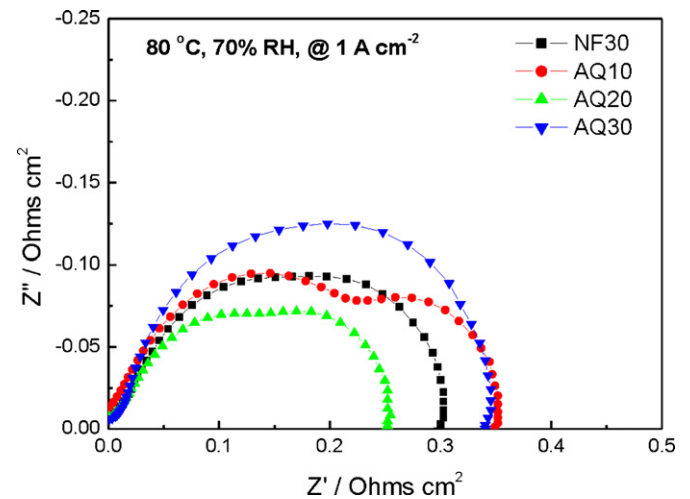


Fig. 11. *In situ* electrochemical impedance spectra obtained at 80 °C and 70% RH while the cell is operated at 1.0 A cm⁻².

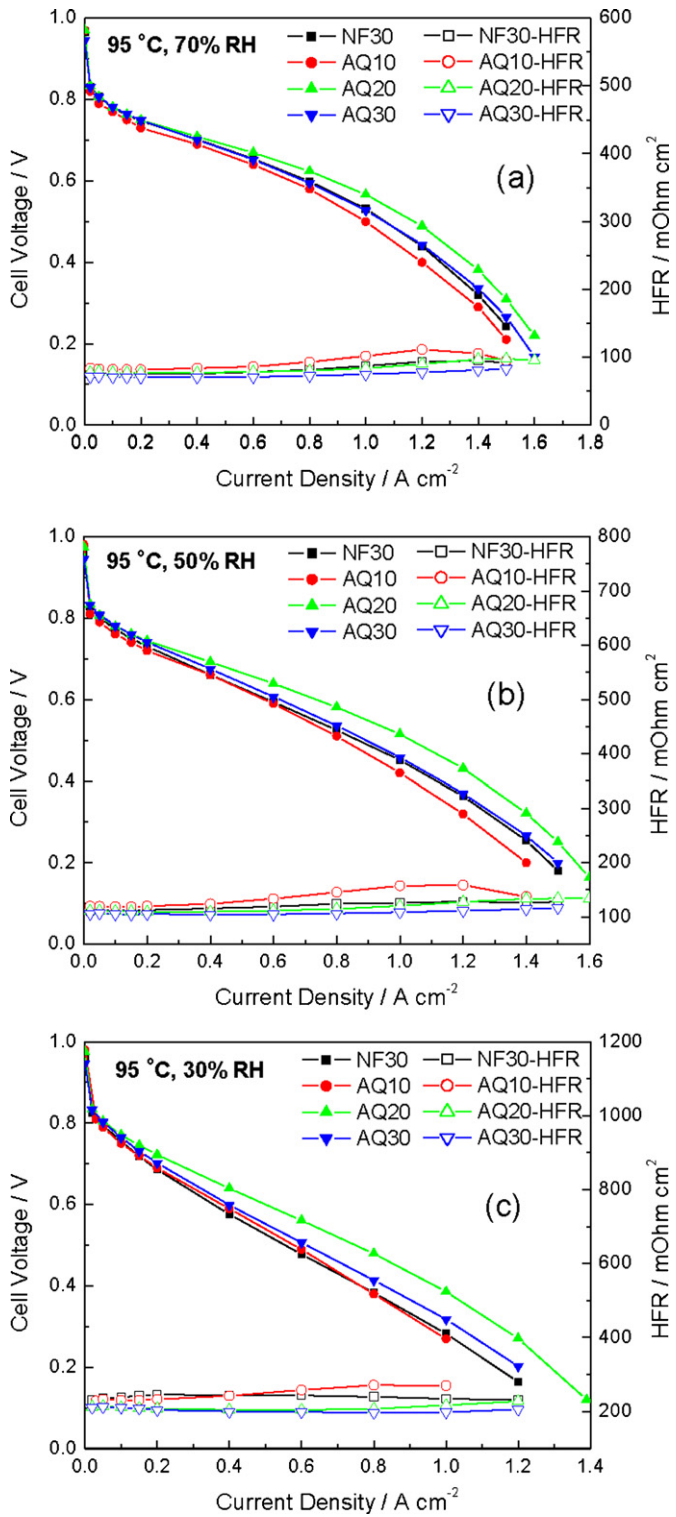


Fig. 12. H₂/air polarization curves at 95 °C and RH values of (a) 70%, (b) 50% and (c) 30%.

(~47%), and displayed a similar low frequency arc in the EIS as AQ20 (porosity ~42%); however, AQ10 exhibited a larger high frequency arc (R_{ct}) due to its high proton resistance inside the CL. Therefore, the total cell resistance of AQ10 became greater than AQ20. In contrast, AQ30 achieved the highest proton conductivity, but showed an even larger total cell resistance due to its small porosity. Overall, as the Aquivion™ content was raised, the proton conductance increased and the porosity of the CL decreased. It is

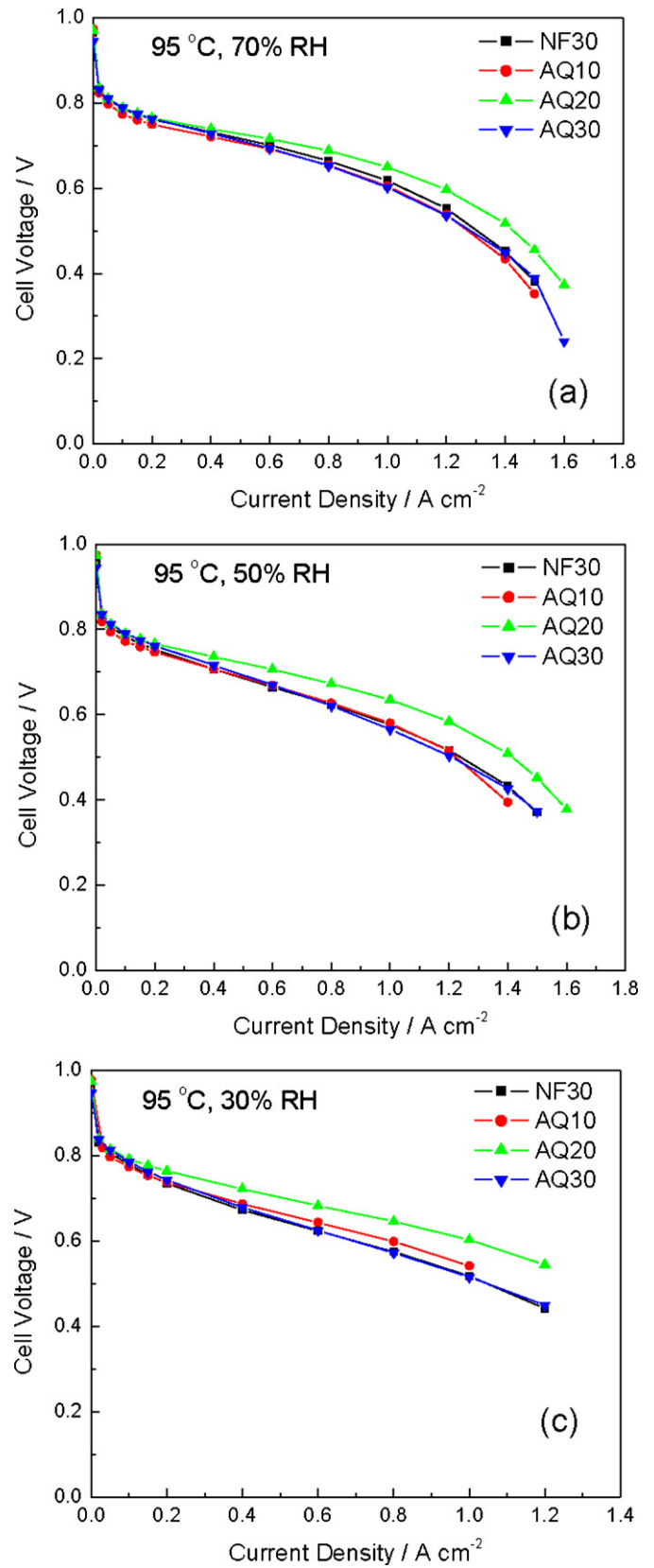


Fig. 13. iR compensated H₂/air polarization curves at 95 °C and RH values of (a) 70%, (b) 50% and (c) 30%.

thus concluded that the higher performance of AQ20 is attributed to an optimal balance between protonic resistance and porosity in the Aquivion™-based MEAs.

H₂/air polarization curves and HFR results for all these MEAs were also obtained at an elevated temperature of 95 °C and at various RHs (Fig. 12). In general, AQ10 demonstrated slightly lower cell voltages, especially at high current densities, which was probably due to its higher HFR. AQ30 showed a similar performance to NF30. Again, AQ20 displayed a superior cell performance amongst the tested MEAs at the increased temperature, with the improvement becoming more pronounced under drier conditions. For example, in comparison to NF30, the cell voltage enhancement of AQ20 at 1.0 A cm⁻² increased to 100 mV at 30% RH.

In order to eliminate the effect of the cell resistance on the polarization curves, the *i*R compensated H₂/air polarization curves are plotted in Fig. 13. AQ10, AQ30 and the baseline sample NF30 exhibited very similar performances. The difference in the measured cell voltage at a given current density among these three MEAs is less than 10 mV. The results suggest that when the conventional Nafion® ionomer is replaced by a low EW ionomer, the ionomer loading can be significantly reduced without sacrificing cell performances under dry conditions. The high hydrophilicity of the SSC ionomer, along with its low EW, may help to retain water and, thus, provide sufficient protonic conductivity under dry conditions, even at ionomer loadings as low as 10 wt%.

4. Conclusions

In summary, fuel cell CCLs containing different loadings of a low EW SSC PFSA ionomer, Aquivion™, were fabricated and investigated in terms of their fuel cell performance and morphology. The results were compared with baseline CCLs prepared using the conventional ionomer 1100 EW Nafion®.

ECSA and C_{dl} of all the SSC ionomer-based samples were similar to those of the baseline. The ORR kinetics of AQ20 and AQ30 under 100% RH were significantly lower than the baseline; however, they were similar to NF30 at 70% RH. *In situ* EIS measurements suggested that the lowered ORR kinetics at 100% RH may be attributed to larger mass transport resistances in SSC-based CCLs compared to the baseline CCLs.

An increase in cell voltage was observed for CCLs containing 20 wt% Aquivion™. The cell performance in AQ20 demonstrated further improvement under dry conditions at 95 °C. For example, relative to the baseline sample, the cell voltage enhancement at 1.0 A cm⁻² of the AQ20 MEA reached 100 mV at 95 °C and 30% RH. These results suggest that even for low ionomer loadings of only

10 wt%, CCLs containing low EW ionomer can achieve performances comparable to baseline CCLs when the cell is operated at 95 °C and under dry conditions. The high hydrophilicity, low EW of these SSC ionomers and more effective use of pore space are believed to account for the improved fuel cell performance.

Acknowledgments

Thanks go to the NRC Technology Development Program for financial support and to Ballard and AFCC for financial and in-kind support. Mr. Paul Le Marquand is thanked for validation of the catalyst ink stability and for proofing this manuscript. Mr. Dave Edwards and Dr. Ken Shi are thanked for technical discussions.

References

- [1] S. Litster, G. McLean, *Journal of Power Sources* 130 (2004) 61–76.
- [2] Z. Xie, T. Navessin, K. Shi, R. Chow, Q.P. Wang, D.T. Song, B. Andreas, M. Eikerling, Z.S. Liu, S. Holdcroft, *Journal of the Electrochemical Society* 152 (2005) A1171–A1179.
- [3] Z. Xie, X.S. Zhao, M. Adachi, Z.Q. Shi, T. Mashio, A. Ohma, K. Shinohara, S. Holdcroft, *Energy and Environmental Science* 1 (2008) 184–193.
- [4] E. Passalacqua, F. Lufrano, G. Squadrito, A. Patti, L. Giorgi, *Electrochimica Acta* 46 (2001) 799–805.
- [5] K.H. Kim, K.Y. Lee, H.J. Kim, E. Cho, S.Y. Lee, T.H. Lim, S.P. Yoon, I.C. Hwang, J.H. Jang, *International Journal of Hydrogen Energy* 35 (2010) 2119–2126.
- [6] E. Antolini, L. Giorgi, A. Pozio, E. Passalacqua, *Journal of Power Sources* 77 (1999) 136–142.
- [7] J. Larminie, A. Dicks, *Fuel Cell Systems Explained*, John Wiley and Sons, Chichester, England, 2000.
- [8] G.A. Eisman, *Journal of Power Sources* 29 (1990) 389–398.
- [9] A. Ghielmi, P. Vaccarono, C. Troglia, V. Arcella, *Journal of Power Sources* 145 (2005) 108–115.
- [10] L. Merlo, A. Ghielmi, L. Cirillo, M. Gebert, V. Arcella, *Separation Science and Technology* 42 (2007) 2891–2908.
- [11] S.J. Paddison, J.A. Elliott, *Solid State Ionics* 178 (2007) 561–567.
- [12] K.D. Kreuer, M. Schuster, B. Obliers, O. Diat, U. Traub, A. Fuchs, U. Klock, S.J. Paddison, J. Maier, *Journal of Power Sources* 178 (2008) 499–509.
- [13] S.J. Paddison, J.A. Elliott, *Solid State Ionics* 177 (2006) 2385–2390.
- [14] D.S. Wu, S.J. Paddison, J.A. Elliott, *Energy and Environmental Science* 1 (2008) 284–293.
- [15] H. Xu, H.R. Kunz, L.J. Bonville, J.M. Fenton, *Journal of Electrochemical Society* 154 (2007) B271–B278.
- [16] J. Peron, D. Edwards, M. Haldane, X.Y. Luo, Y.M. Zhang, S. Holdcroft, Z.Q. Shi, *Journal of Power Sources* 196 (2011) 179–181.
- [17] V. Arcella, C. Troglia, A. Ghielmi, *Industrial and Engineering Chemistry Research* 44 (2005) 7646–7651.
- [18] F.E. Hizir, S.O. Ural, E.C. Kumbur, M.M. Mench, *Journal of Power Sources* 195 (2010) 3463–3471.
- [19] M.P. Manahan, S. Kim, E.C. Kumbur, M.M. Mench, *ECS Transactions* 25 (2009) 1745–1754.
- [20] H. Xu, R. Kunz, J.M. Fenton, *Electrochemical Solid State Letters* 10 (2007) B1–B5.
- [21] K.C. Neyerlin, H.A. Gasteiger, C.K. Mittelstaedt, J. Jorne, W.B. Gu, *Journal of Electrochemical Society* 152 (2005) A1073–A1080.